Frequency Tunable Non-Reciprocal Bandpass Filter Using Time-Modulated Microstrip $\lambda_g/2$ Resonators

Xiaohu Wu [ID], *Senior Member, IEEE*, Mahmoud Nafe, *Graduate Student Member, IEEE*,
Alejandro Álvarez Melcón [ID], *Senior Member, IEEE*, Juan Sebastián Gómez-Díaz [ID], *Senior Member, IEEE*,
and Xiaoguang Liu [ID], *Senior Member, IEEE*

Abstract—This brief presents a novel frequency reconfigurable microstrip non-reciprocal bandpass filter based on time-modulated microstrip $\lambda_g/2$ resonators. The modulation is achieved by loading both ends of the $\lambda_g/2$ transmission line resonators with time-modulated capacitors. The modulation voltage source is connected at the center of the resonator, where there is a natural voltage null, and a single inductor is used to further enhance the biasing isolation. The wideband nature of this isolation scheme enables the tuning of the devices over a wide frequency range. With more than 30-dB RF to modulation isolation, the proposed resonator structure also enables low insertion loss by eliminating RF signal leakage to the modulation ports. A 3-pole bandpass filter example is simulated and measured, showing a minimal insertion loss of 3.9 dB, a 20-dB isolation bandwidth of 42 MHz at 1.0 GHz, and frequency tuning range of 885–1031 MHz.

Index Terms—Bandpass filter (BPF), isolator, microstrip, magnetless, non-reciprocal, time-invariant, time-modulated, tunable.
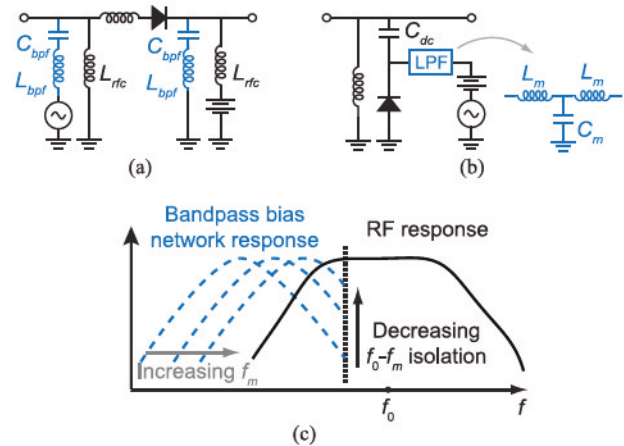
Fig. 1. Reported varactor-based time-varying resonators. (a) Time-varying serial LC resonator with individual BPF and dc bias circuits [3]. (b) Time-varying parallel LC resonator with LPF bias circuit and a single dc block capacitor C_{dc} [7]. (c) A conceptual illustration for bias limitation at larger f_m. Frequency f_0 is the RF passband center frequency.

I. INTRODUCTION

NON-RECIPROCAL components, such as circulators and isolators, are important devices in wireless communication systems, either for protecting active blocks from the unwanted reflections or enabling full-duplex communications [1]. Conventional designs of these devices rely on the

Xiaohu Wu is with the School of Electronic and Information Engineering, Nanjing University of Information Science and Technology, Nanjing 210044, China, and also with the Department of Electrical and Computer Engineering, University of California at Davis, Davis, CA 95616 USA (e-mail: wxhwu@ucdavis.edu).

Mahmoud Nafe, Juan Sebastián Gómez-Díaz, and Xiaoguang Liu are with the Department of Electrical and Computer Engineering, University of California, Davis, Davis, CA 95616 USA (e-mail: manafe@ucdavis.edu; jsgomez@ucdavis.edu; lxgliu@ucdavis.edu).

Alejandro Álvarez Melcón is with the Department of Information and Communication Technologies, Technical University of Cartagena, 30202 Murcia, Spain (e-mail: alejandro.alvarez@upct.es).

Color versions of one or more of the figures in this article are available online at https://ieeexplore.ieee.org.

Digital Object Identifier 10.1109/TCSII.2020.3014499

ferrite materials, which are bulky, expensive, and incompatible with integrated circuits.

Recently, linear periodically time-varying (LPTV) circuits have been proposed as a new approach to achieve magnetless non-reciprocity. Magnetless circulators are implemented by spatiotemporally modulating three lumped-element LC resonators connected either in a Δ or Y topology [2], [3]. Extension works in the same rationale are reported in [4], [5]. Magnetless circulator can also be realized by embedding gyrators of 180° non-reciprocal phase inside a $3/4\lambda_g$ ring resonator [6].

In [7], a non-reciprocal BPF (isolator) and its full-spectra analysis are reported by using spatio-temporal modulation of a lumped-element coupled-resonator filter at 0.19 GHz. The analysis is then generalized to a time-varying coupling matrix approach in [8]. Non-reciprocal 140-MHz-centered BPF using lumped LC elements is also presented in [9]. In [10], the modulation sources of the non-reciprocal microstrip BPF are directly loaded to the RF resonators, leading to a weak f_m-f_{RF} isolation of around 10 dB. As a result, the 5.5-dB insertion loss (*IL*) and the spurious even-mode resonances significantly deteriorate the filtering performances.

In this brief, we propose a magnetless non-reciprocal BPF based on time-modulated microstrip resonators of simple and

effective biasing scheme. With the help of a single inductor, a wideband 30-dB f_m-f_{RF} isolation can be achieved by taking advantage of the voltage null point at the center of $\lambda_g/2$ resonators. The high f_m-f_{RF} isolation not only eliminates the spurious resonances but also results in less RF leakage and thus a lower forward IL of 3.9 dB. We also demonstrate frequency tuning capabilities in the non-reciprocal BPF. A 3-pole non-reciprocal BPF is designed, fabricated, and measured.

II. TIME-VARYING RESONATORS

A. Review of Reported Time-Varying Resonators

Existing works on spatio-temporal modulation (STM) based non-reciprocal components are predominantly based on modulating lumped-element resonators [2], [3], [7]. Both series resonators [Fig. 1 (a)] and shunt resonators [Fig. 1 (b)] have been used. A key design challenge in these time-varying resonators lies in separating the RF and modulation signals. This is usually achieved by duplexing circuits. In Fig. 1 (a), for example, C_{bpf} and L_{bpf} constitute a bandpass filter (BPF) centered at the modulation frequency f_m to prevent the RF signal from leaking into the modulation voltage source. Because the BPF also blocks the dc bias voltage, an additional dc return pass is provided by a large inductor L_{rfc} as an RF choke. Similarly, in Fig. 1 (b), the modulation voltage source is isolated by a low-pass filter (LPF) and a static dc-blocking capacitor C_{dc}. Obviously, in a practical implementation, the addition of the bias and duplexing circuits will add to the insertion loss of the overall circuit.

In addition, it is important to realize that f_m is approximately equal to the inherent static RF bandwidth (BW) of the non-reciprocal filter [7]. A larger static BW together with higher f_m can provide wider non-reciprocal bandwidth. As a result, the cut-off frequency of the duplexing circuit must also be increased to accommodate the larger f_m, which in turn will reduce the rejection level at the RF frequency. Taking the bandpass biasing case as an example, as shown in Fig. 1 (c), the bandpass biasing attenuation at the non-reciprocal passband frequency f_0 decreases with the increase of f_m, leading to more RF leakage to the modulation sources. The same situation can be found in the lowpass bias case. This can be solved by increasing the order of the biasing bandpass or lowpass filters to have higher roll-off, although at the cost of increased circuit complexity and higher insertion loss of the overall circuit.

B. Proposed Distributed Time-Varying Resonator

To overcome the above difficulties of lumped-element resonators, we propose a distributed time-varying resonator as shown in Fig. 2. To modulate the resonant frequency, the microstrip resonator is symmetrically loaded by varactors at both two ends. The modulating wave is applied at the center of the resonator which is a virtual ground at f_0 but not at f_m. As a result, the proposed time-varying distributed resonator can realize inherent isolation between the RF signal and the modulation signal.

1) Resonant Frequency: Due to the symmetry of the $\lambda_g/2$ resonator, its resonant frequency can be analyzed by its odd-mode circuit shown in Fig. 2 (b). The input admittance of the
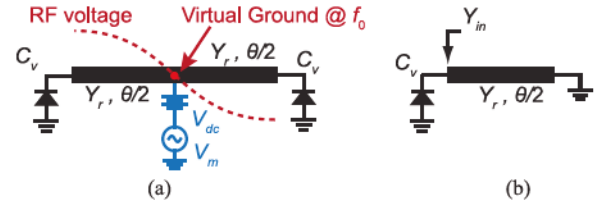

Fig. 2. (a) Resonant structure of the proposed time-varying microstrip $\lambda_g/2$ resonator. C_v is the equivalent capacitance of the reversely biased varactor. f_0 is the resonant frequency and also the filter passband center frequency. (b) Odd-mode equivalent circuit.
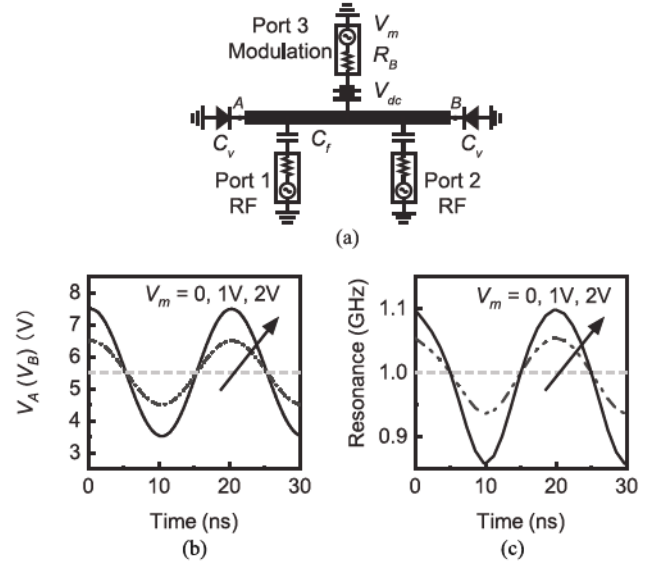

Fig. 3. (a) Proposed time-modulated resonator with weak external coupling of $C_f = 0.003$ pF to extract the time-variant resonant frequency. (b) Extracted biasing voltage at the loading point A and B. (c) Extracted time-varying resonant frequency with respect to the modulation amplitude V_m. Here, $V_{dc} = 5.5$ V and $R_B = 50\,\Omega$.

odd-mode circuit is

$$Y_{in} = j(\omega C_v - Y_r \cot\frac{\theta}{2}). \tag{1}$$

The resonant frequency f can be solved by setting $I_m\{Y_{in}\} = 0$,

$$f = \frac{Y_r}{2\pi C_v}\cot\frac{\theta}{2}. \tag{2}$$

In this brief, an 80-Ω transmission line with $\theta = 80°$ and an equivalent static capacitance of 2.3 pF are chosen for a nominal (static) resonant frequency of 1.0 GHz. Skyworks SMV1234 varactors are used to modulate the resonator. The nominal capacitance of 2.3 pF is achieved at a reversely biased *dc* voltage of 5.0 V [11].

The resonant frequency can be modulated by modulating the varactors with a sinusoidal voltage V_m. Fig. 3 (a) shows the simulation setup to study the time-varying resonant properties of the proposed resonator. The resonator is weakly coupled to the source and the load by two 0.003-pF capacitors. Harmonic balance in Keysight Advanced Design System (ADS) is used to extract the biasing voltage and time-varying resonant frequency [Fig. 3 (b) and (c)]. Here, a 50-MHz sinusoidal wave with phase $\phi = 0°$ and various
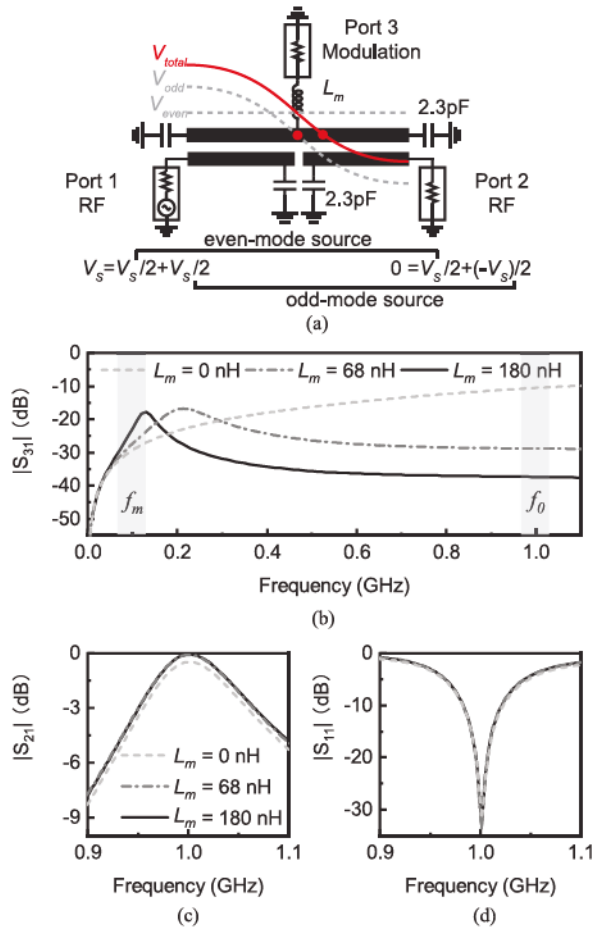
Fig. 4. (a) Circuit simulation setup to study the f_m-f_{RF} isolation of the time-varying resonator. V_{even}, V_{odd}, and V_{total} are the even mode, odd mode, and total waveform, respectively. The even- and odd-mode impedance of the coupled line are set to 90 Ω and 50 Ω, respectively. (b) Simulated f_m-f_{RF} isolation ($|S_{31}|$). (c) Simulated RF transmission $|S_{21}|$. (d) Simulated RF reflection $|S_{11}|$. Legend of (d) is removed for clarity, lines correspond to the same investigated inductor values as (b) and (c).

amplitude V_m is used as the modulation waveform. The resonance is time-invariant when $V_m = 0$ V, which is the case without time-modulation. Higher V_m results in a larger modulation on the resonance. Note that the resonant frequency is nonlinear with respect to the modulation waveform due to the nonlinearity of (2) and the varactor's nonlinear *C–V* characteristics [11].

2) Bias Isolation: With the modulation circuitry connected to the center of the $\lambda_g/2$ resonator, an inherent isolation between the bias signal and the RF signal is provided. If the resonator is under an odd mode excitation, the RF signal is ideally isolated from the bias signal due to the symmetry of the structure [Fig. 2 (a)]. In an actual filter, however, the resonators are usually not excited with an ideal differential waveform. The setup of Fig. 4 (a) is used to understand the f_m-f_{RF} isolation through static S-parameter simulations. For simplicity, the *dc*-biased 2.3-pF varactors are replaced by lossless capacitors to exclude the varactor loss and show the leakage loss. The end-loading capacitances at the feed lines are selected to be close to the varactor capacitance to have proper coupling of the parallel-coupled line for RF signals [1]. In S-parameter
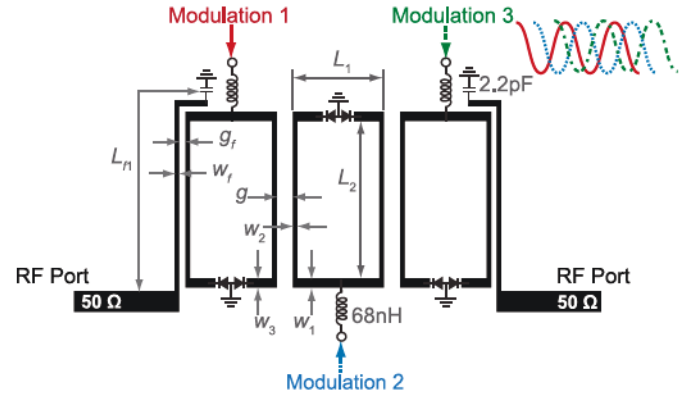

Fig. 5. Microstrip layout of the proposed filter.

simulation, all ports are matched while one of the ports (e.g., Port 1) is excited with a source. As such, the excitation is a combination of odd mode and even mode sources. Due to the existence of the even mode effect, the voltage on the $\lambda_g/2$ resonator is not ideally symmetric, leading to a non-perfect isolation. In fact, Fig. 4 (b) shows that only 10-dB f_m-f_{RF} isolation can be achieved at f_0. Such a weak biasing isolation results in a strong loading effect of the modulation circuit on the even-mode resonances and introduces undesired spurious responses [10].

To provide an enhanced isolation, additional LPF can be inserted at the modulation port. A simple implementation takes the form of a series inductor L_m. Fig. 4 (b) shows the f_m-f_{RF} isolation for various L_m values. An L_m value of 68 nH can improve the isolation at f_{RF} by almost 20 dB. Isolation at f_m remains the same at 35 dB. Note that $|S_{31}|$ is equal to $|S_{32}|$ due to the symmetry and that the isolation between both the RF ports and the modulation port is very good. The enhanced f_m-f_{RF} isolation also leads to lower RF transmission IL between the two RF ports. As seen in Fig. 4 (c) and (d), the model in Fig. 4 (a) has a passband centered at 1.0 GHz. Due to the f_{RF} leakage to the modulation branch, 0.66-dB IL can be observed from the filter transmission coefficient $|S_{21}|$ when $L_m = 0$. With an inductor L_m of 68 nH, a 0.38-dB improvement of IL can be attained.

Although a small f_m value is used in this brief, the depicted isolation behaviour of Fig. 4 (b) indicates that larger f_m values are also as effective. This property may benefit other applications, such as high-performance circulators. For example, spatio-temporal modulation based circulators using larger f_m have lower transmission IL, smaller intermodulation products, better port matching, and larger separation between the desired RF signal and the intermodulation products [3].

III. APPLICATIONS AND RESULTS

Non-reciprocal BPF using the proposed time-modulated $\lambda_g/2$ resonators is presented in this section. The filter is designed on Rogers 4003C substrates with a thickness of 0.813 mm, a relative permittivity of 3.55, and a loss tangent of 0.0027. The design of non-reciprocal BPF can start with designing a conventional reciprocal BPF of static specifications. The final non-reciprocal filtering performances can be achieved by applying proper time-modulation [7].
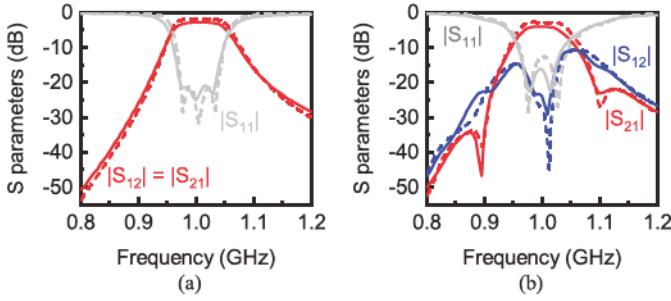
Fig. 6. Simulation and measurement results. Solid line: measurement. Dash line: simulation. (a) Non-modulated reciprocal responses. (b) Modulated Non-reciprocal responses.

TABLE I
PARAMETERS OF THE TUNING STATES

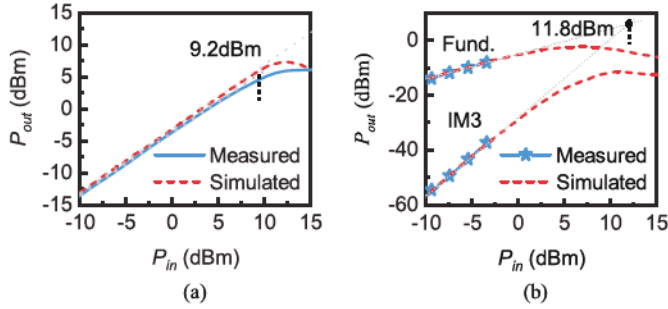|	T1	T2	T3	T4
V_{dc}	4.2 V	5.2 V	6.0 V	7.2 V
f_m	57 MHz	61 MHz	65 MHz	72 MHz
V_m	0.65V	0.80V	1.1V	1.35V
$\Delta\varphi$	45°	45°	45°	45°
f_0	885 MHz	954 MHz	1000 MHz	1031 MHz
IL	4.6 dB	4.2 dB	3.9 dB	3.9 dB
BW_{IX}	44 MHz	44 MHz	42 MHz	43 MHz
RL	> 10.9 dB	> 15.9 dB	> 16.1 dB	> 15.1 dB

Fig. 7. Power handling and nonlinearity characterization. (a) Simulated and measured P1dB with a single-tone signal at 1.0 GHz. (b) Simulated and measured IIP3 with a two-tone signal centered at 1.0 GHz and separated by 20 MHz.

A. Non-Reciprocal Filter And Results

The corresponding static filter is specified to be centered at 1.0 GHz with a Chebyshev response having a passband ripple of 0.04 dB and a ripple bandwidth of 60 MHz. The design parameters, namely the coupling coefficient M_{ij} and the external quality factor Q_e, can be obtained as $M_{12} = M_{23} = 0.062$ and $Q_e = 14.2$ [12].

The layout of the 3-pole filter is shown in Fig. 5. The three time-modulated microstrip resonators of ring configuration are in-line coupled to each other. The resonator strip width along the coupling side is slightly reduced to provide larger coupling to meet the bandwidth requirement [12]. The resonator dimensions are $L_1 = 7.80$ mm, $L_2 = 13.42$ mm, $w_1 = 0.80$ mm, $w_2 = 0.40$ mm, and $w_3 = 0.80$ mm. Accordingly, V_{dc} is adjusted from 5.0 V (Section II-B) to 6.0 V here to fine tune the resonance at 1.0 GHz. The dimensions of the coupling structures, g for M_{12} (M_{23}) and L_{f1}, g_f, and w_f for Q_e, can be extracted by conventional filter design method [12]. The gap width g is chosen to be 0.77 mm to realize an M_{12} (M_{23}) of 0.062. The other parameters $w_f = 0.4$ mm, $L_{f1} = 18.3$ mm, and $g_f = 0.17$ mm are chosen to realize a Q_e of 14.2.

The simulated and measured results of the static 3-pole filter are shown in Fig. 6 (a). Without modulation, the static filter exhibits a conventional reciprocal 3-pole Chebyshev passband at 1.0 GHz. It has an IL of 2.6 dB and a 3-dB bandwidth of 96 MHz. The 2.6-dB IL is mainly due to the varactor loss and conductor loss, and is comparable to these varactor-loaded filters, e.g., 2.8 dB in [8]. The return loss (RL) is better than 20 dB across the passband.

Next, to achieve a non-reciprocal BPF performance, time-modulation with incremental phase $\Delta\varphi = 45°$ is applied [7]. The modulation frequency $f_m = 65$ MHz is close to the static ripple bandwidth and V_m is optimized to 1.1 V. The resulting non-reciprocal responses are shown in Fig. 6 (b), where two isolation poles and two reflection poles can be observed in both simulation and measurement. The measured forward IL ($|S_{21}|$) is 3.9 dB, which is 1.3-dB higher than the static case. This is mainly due to the power conversion to the intermodulation (IM) frequencies [7], [8]. The measured backward isolation (IX) is 23.2 dB at the center frequency 1.0 GHz, i.e., $IX_{f_0} = 23.2$ dB. The measured 20-dB IX bandwidth is 978–1020 MHz, i.e., $BW_{IX} = 42$ MHz. The measured RL across the 20-dB isolation bandwidth is better than 16.1 dB.

Interestingly, the modulating state in Fig. 6 (b) becomes a quasi-elliptic response with two transmission zeros at 895 MHz and 1100 MHz, respectively. These two transmission zeros are the results of "cross coupling" in the time-modulated network. Here, unlike in conventional filter designs that cross coupling is introduced by two or more intentionally designed physical signal paths, the cross coupling in a time-modulated network is created because of the RF signal cancellation between these multiple conversion paths with IM frequencies (RF-IM-RF) and the main RF-RF transmission path [7], [8].

Fig. 7 shows the simulated and measured input-referred 1-dB compression point (P1dB) and the input-referred third-order intercept point (IIP3). The measured P1dB is 9.2 dBm and the measured IIP3 is 11.8 dBm. The linearity and power handling of the non-reciprocal filter may be improved by using stacked diodes configurations [13].

B. Frequency Tunability

Frequency tunability is of great interest to future wireless communications and sensing systems for better utilization of the limited frequency spectrum resources. The proposed non-reciprocal filter can be tuned by changing the bias dc voltage (V_{dc}) and the modulation parameters (f_m and V_m). Fig. 8 (a)–(c) in the next page show the tuning S-parameter profiles of the proposed filter. Specifically, it can be tuned from 885 MHz to 1031 MHz with two distinct isolation poles [Fig. 8 (b)] and two reflection poles [Fig. 8 (c)] in all the tuned states. The smaller IL at higher f_0 is due to the lower parasitic resistance of the varactor at higher V_{dc} [11].

Larger f_m as well as higher V_m in Table I are used to achieve non-reciprocity at higher f_0. This is because the corresponding filter has wider static transmission bandwidth at higher
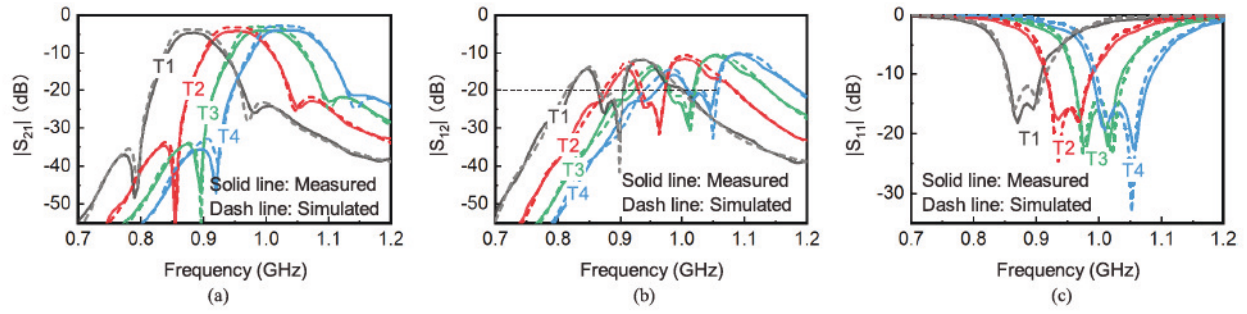
Fig. 8. Simulated and measured frequency tuning characteristics of the proposed non-reciprocal filter. (a), (b), and (c) are the tuned $|S_{21}|$, $|S_{12}|$, and $|S_{11}|$, respectively. Although only a few discrete states T1, T2, T3, and T4 are shown, the non-reciprocal filter can be continuously tuned.

TABLE II
COMPARISON BETWEEN THIS BRIEF AND REPORTED WORKS

Device	[5] Circulator	[7] Isolator	[8] Isolator	This work Isolator
Technology	Lumped	Lumped	Microstrip	Microstrip
f_0 (GHz)	1.0	0.19	0.96	1.0
IL (dB)	2.0	1.5	4.5	3.9
ΔIL (dB)	N/A	0.7	1.7	1.3
RL (dB)	20	15.0	N/A	16.1
IX_{f_0} (dB)	24	20.2	18.3	23.2
BW_{IX} (MHz)	23	20	N/A	42
TZs	0	0	1	2
k_{rc}	N/A	0.29	0.36	0.55

TZs: transmission zeros. k_{rc}: passband rectangle coefficient defined as the ratio of 3-dB bandwidth over 20-dB bandwidth. ΔIL: IL degradation due to modulation.

f_0 due to the frequency-dependent nature of the distributed coupling [12]. To have a wider tunable range of constant passband bandwidth BW, the frequency-curve shape design method in [14] and the coupling matrix based extraction technique in [15] have been newly developed. Such ideas may be used in the future to improve the tuning performances of the non-reciprocal filters.

C. Comparison With Previous Works

Table II compares the proposed work and some of these reported works. Reference [5] demonstrates a three-port circulator in a differential modulation form to enhance all the metrics except that it has a passband of gradual roll-off and 10-dB stopband rejection ([5, Fig. 9]). Two-port lumped non-reciprocal BPF in [7] has lower IL and lower IL degradation due to the modulation (ΔIL), due to the higher quality factor of the varactors at the designed lower frequency 0.19 GHz. The complicated non-planar modulation design in [8] leads to sub-optimal filter responses, i.e., 4.5-dB IL, 1.7-dB ΔIL, and sub-20-dB IX. In contrast, this brief proposes a non-reciprocal filter using microstrip resonator with a simpler and more efficient biasing strategy. It has an IL of 3.9 dB and a BW_{IX} of 42 MHz at $f_0 = 1.0$ GHz. Moreover, two reflection poles, two isolation poles, two transmission zeros, and higher stopband rejection (i.e., larger k_{rc}) can be observed in this brief, showing superior filtering and isolation performances.

IV. CONCLUSION

This brief introduces a novel distributed non-reciprocal filter using time-modulated microstrip $\lambda_g/2$ resonators. The filter is of simple biasing configuration and achieves excellent non-reciprocal filtering performances, by proposing a new biasing scheme for the modulation signals. The effectiveness of the proposed ideas is well validated by the close agreement between the measurement and simulation results.

REFERENCES

[1] D. M. Pozar, *Microwave Engineering*. New Delhi, India: Wiley, 2012.
[2] N. A. Estep, D. L. Sounas, J. Soric, and A. Alù, "Magnetic-free non-reciprocity and isolation based on parametrically modulated coupled-resonator loops," *Nat. Phys.*, vol. 10, pp. 923–927, Dec. 2014.
[3] N. A. Estep, D. L. Sounas, and A. Alù, "Magnetless microwave circulators based on spatiotemporally modulated rings of coupled resonators," *IEEE Trans. Microw. Theory Techn.*, vol. 64, no. 2, pp. 502–518, Feb. 2016.
[4] A. Kord, D. L. Sounas, Z. Xiao, and A. Alù, "Broadband cyclic-symmetric magnetless circulators and theoretical bounds on their bandwidth," *IEEE Trans. Microw. Theory Techn.*, vol. 66, no. 12, pp. 5472–5481, Dec. 2018.
[5] A. Kord, D. L. Sounas, and A. Alù, "Pseudo-linear time-invariant magnetless circulators based on differential spatiotemporal modulation of resonant junctions," *IEEE Trans. Microw. Theory Techn.*, vol. 66, no. 6, pp. 2731–2745, Jun. 2018.
[6] N. Reiskarimian and H. Krishnaswamy, "Magnetic-free non-reciprocity based on staggered commutation," *Nat. Commun.*, vol. 7, Apr. 2016, Art. no. 11217.
[7] X. Wu, X. Liu, M. D. Hickle, D. Peroulis, J. S. Gómez-Díaz, and A. Álvarez Melcón, "Isolating bandpass filters using time-modulated resonators," *IEEE Trans. Microw. Theory Techn.*, vol. 67, no. 6, pp. 2331–2345, Jun. 2019.
[8] A. Álvarez Melcón, X. Wu, J. Zang, X. Liu, and J. S. Gómez-Díaz, "Coupling matrix representation of nonreciprocal filters based on time-modulated resonators," *IEEE Trans. Microw. Theory Techn.*, vol. 67, no. 12, pp. 4751–4763, Dec. 2019.
[9] D. Simpson and D. Psychogiou, "Magnet-less Non-reciprocal bandpass filters with tunable center frequency," in *Proc. 49th Eur. Microw. Conf.*, Paris, France, Oct. 2019, pp. 460–463.
[10] X. Wu, M. Nafe, A. Álvarez Melcón, J. S. Gómez-Díaz, and X. Liu, "A non-reciprocal microstrip bandpass filter based on spatio-temporal modulation," in *Proc. IEEE MTT-S Int. Microw. Symp. (IMS)*, Boston, MA, USA, Jun. 2019, pp. 9–12.
[11] *SMV123x Series: Hyperabrupt Junction Tuning Varactors*, Skyworks Solutions, Inc., Irvine, CA, USA, Nov. 2018.
[12] J.-S. Hong and M. J. Lancaster, *Microstrip Filters for RF/Microwave Applications*. New York, NY, USA: Wiley, 2001.
[13] K. Buisman *et al.*, "Varactor topologies for RF adaptivity with improved power handling and linearity," in *Proc. IEEE/MTT-S Int. Microw. Symp.*, Honolulu, HI, USA, Jun. 2007, pp. 319–322.
[14] M. Ohira, S. Hashimoto, Z. Ma, and X. Wang, "Coupling-matrix-based systematic design of single-DC-bias-controlled microstrip higher order tunable bandpass filters with constant absolute bandwidth and transmission zeros," *IEEE Trans. Microw. Theory Techn.*, vol. 67, no. 1, pp. 118–128, Jan. 2019.
[15] D. Lu, M. Yu, N. S. Barker, Z. Li, W. Li, and X. Tang, "Advanced synthesis of wide-tuning-range frequency-adaptive bandpass filter with constant absolute bandwidth," *IEEE Trans. Microw. Theory Techn.*, vol. 67, no. 11, pp. 4362–4375, Nov. 2019.